Available online at www.sciencedirect.com

ScienceDirect

IFAC PapersOnline CONFERENCE PAPER ARCHIVE

IFAC PapersOnLine 55-27 (2022) 1–6

WEC Array Optimization with Multi-Resonance and Phase Control of Electrical Power Take-Off ⋆

Madelyn G. Veurink * **Wayne W. Weaver** *
Rush D. Robinett III * **David G. Wilson** **
Ronald C. Matthews **

* *Michigan Technological University, Houghton, MI 49931, USA (e-mail: mgveurin,wwweaver,rdrobine@mtu.edu).*
** *Sandia National Labs, Albuquerque, New Mexico 87123, USA (e-mail: dwilso,rcmatth@sandia.gov)*

Abstract: This new research provides transformative marine energy technology to effectively power the blue economy. Harmonizing the energy capture and power from Wave Energy Converter (WEC) arrays require innovative designs for the buoy, electric machines, energy storage systems (ESS), and coordinated onshore electric power grid (EPG) integration. This paper introduces two innovative elements that are co-designed to extract the maximum power from; i) individual WEC buoys with a multi-resonance controller design and ii) synchronized with power packet network phase control through the physical placement of the WEC arrays reducing ESS requirements. MATLAB/Simulink models were created for the WEC array dynamics and control systems with Bretschneider irregular wave spectrum as inputs. The numerical simulation results show that for ideal physical WEC buoy array phasing of 60 degrees the ESS peak power and energy capacity requirements are minimized while the multi-resonant controllers optimize EPG power output for each WEC buoy.

Keywords: Marine Renewable Energy, Energy Harvesting, Motion control, Wave energy converters, Multi-resonance control

1. INTRODUCTION

New developments in transformative marine energy technologies (METs) are needed to help meet the global demands for reduced carbon emission in generation sources (Copping et al., 2020). To harmonize the mix of renewable energy sources from wind, solar, and wave energy; advancements in energy capture and integration with the electric power are a prerequisite. Among these renewable energy resources wave energy is the most recent and less mature. To make WECs economical they must maximize the energy conversion from wave to wire (Song et al., 2016). There is a colossal amount of potential energy within the world's oceans. The United States alone has 2640 TWh beyond the perimeter of its shores (Jacobson et al., 2011). WECs need to be precisely developed and employed to extract this large potential of energy for efficient conversion of useable electricity.

METs will need advances in control systems, power electronics, and architectures for onshore integration of electric power. These renewable energy sources (RES) are stochastic in nature. Traditional methods require ESS with additional power electronic components to provide constant suitable power quality. This comes with increased complexity. Grid stability and resiliency are still relatively new features to be exploited by power converters and will need to stabilize and harmonize the mix of RES to loads. These systems are continually being pushed to higher levels of sophisticated energy management functionality (Chen and Poor, 2020). New METs will benefit from power packetized networked (PPN) enabled microgrids which are becoming viable and effective solutions for RES integration (Chen and Poor, 2020). The smart grid will need to ideally shift from conventional constant voltage and frequency synchronous operations to future asynchronous PPN routing architectures. To optimize the full benefits of a microgrid solution, energy must be able to be freely traded and exchanged between sources and loads with economic incentives (Chen and Poor, 2020). For example, in (Takahashi et al., 2016), a power regulation algorithm was designed to address the load requirement of a dispatching PPN. The stability of the system with a predictive dynamic quantizer in a dispatching PPN was confirmed analytically as a switched system. It was

⋆ This study was funded by the Laboratory Directed Research Development (LDRD) program at Sandia National Laboratories. Sandia National Laboratories is a multi-mission laboratory managed and operated by National Technology and Engineering Solutions of Sandia, LLC., a wholly owned subsidiary of Honeywell International, Inc., for the U.S. Department of Energy's National Nuclear Security Administration under contract DE-NA0003525. This paper describes objective technical results and analysis. Any subjective views or opinions that might be expressed in the paper do not necessarily represent the views of the U.S. Department of Energy or the United States Government. Special thanks to Dr. Ray Byrne at Sandia, for his technical review and programmatic leadership for this LDRD project.

10.1016/j.ifacol.2022.10.479

verified, with both numerical and experimental results, that simultaneous voltage demands from multiple loads in the dispatching PPN were satisfied with this regulation method (Takahashi et al., 2016). The revelation of new functionality in PPNs will become more attractive for large-scale adoption and cost reduction while preserving reliability and resiliency for the future smart grid.

METs such as WECs, receive oscillating wave inputs that need ESS at both the buoy and grid interfaces, respectively. When waves impact the WEC at their resonance frequency, the device absorbs significant amounts of energy efficiently. However, when the WEC is off-resonance with the incoming waves the WECs energy capture is much less efficient. This requires additional; filtering, frequency tuning, power electronics, and ESS to meet the reactive power requirements (Weaver et al., 2020). Two innovative elements identified in this research to aide in the extraction of the maximum power are, i) the design of a multi-resonance controller for each individual WEC buoy and ii) power synchronization that utilizes PPN for phase control through the physical placement of the WEC within the array cluster that reduces the ESS requirements. To maximize the power injected to the grid the control system of the WEC must maximize the energy absorbed by the buoy. The power take off (PTO) mechanisms convert mechanical motion to usable electric energy for each WEC buoy in the array cluster. A rack-and-pinion mechanism performs the conversion from mechanical linear-to-rotational motion which in turn drives the electrical machines. This rotational velocity turns the electrical machines attached to the buoy (Weaver et al., 2020). In (Wilson et al., 2018) the ac power from the electric machine is converted to DC by an AC-to-DC inverter before it is stored in a constant DC bus. The DC power is transmitted to shore by undersea cable and then injected into the electric power grid.

To be economically viable the WEC controls must optimize extracted energy at multiple frequencies across the wave spectrum (Song et al., 2016), (Wilson et al., 2017), (Abdelkhalik et al., 2017a), represented as a Bretschneider Spectrum. There are many different control strategies developed for WECs operating in a single Degree-of-Freedom (DOF). One of these strategies, Complex Conjugate Control (C3), provides the criteria necessary for maximum energy extraction from the WEC in the frequency domain (Fusco and Ringwood, 2012). The two criteria to be met to implement C3 are resonating the natural frequencies of the system with the wave excitation force and adding damping that is equal in magnitude to the system's damping (Falnes and Kurniawan, 2020). A PPN is introduced to efficiently integrate several WECs in an array to the onshore EPG while minimizing the ESS (Veurink et al., 2022).

A time domain C3 control, developed in (Song et al., 2016; Wilson et al., 2017) calculates the phase and magnitudes of the decomposed frequency components of the wave spectrum. This algorithm is realized by creating a proportional derivative (PD) feedback loop for each of the decomposed frequencies from the measured signal (Song et al., 2016), (Wilson et al., 2017). The proportional gain of this controller is calculated using each of the decomposed frequencies which satisfies the C3 criteria. The derivative gain is set equal to the real part of the mechanical impedance (Bacelli, 2014) which can be defined as PDC3.

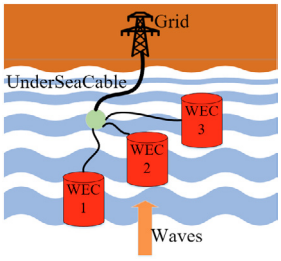

Fig. 1. Three phased WEC array with common collection and undersea cable to grid point of common coupling.

In this research a multi-resonance and phase control methodology is introduced for the electrical PTO to efficiently integrate several WECs in an array to onshore EPG. The ESS is minimized while leveraging the WEC physical location with respect to the incoming waves to allow for increased power capture and power quality through phasing the inputs on a collection bus. In Section 2, the modeling and control of the WEC array is presented. In Section 3 a brief simulation example is shown that illustrates the benefits of utilizing the presented optimization and control strategies. In the last Section 4, summary and conclusions are given.

2. WEC ARRAY MODELING AND CONTROL

A WEC system is composed of a buoy, an electric machine, an energy storage system, a line to shore, and the electric grid integration. To create an array of WECs multiple buoys with electric machines on them are connected to a shared energy storage system. The phased positioning of the buoys in a WEC array relative to the on shore electric grid is shown in Fig. 1.

The electrical PTO of the WECs is shown in Fig. 2. The mechanical system of the WEC absorbs the power in the waves and the electrical system of each buoy in an array injects the generated power into the bus as i_{pto}. For an array of multiple WECs the buoys are connected to the substation in a parallel configuration. The electrical PTO for the WECs is based off of previous work done in (Weaver et al., 2020).

2.1 Mechanical Drive-Train

The mechanical system of the WEC array is modeled as a mass-spring-damper differential equation

$$m\ddot{x}_i + c_i\dot{x}_i + kx_i = f_{e,i} + f_{u,i}. \tag{1}$$

The control force on each buoy in the WEC array, f_{ui}, has the same time shift as the excitation force acting on the respective WEC. The control force is replaced by the linear force of the three permanent magnet DC machines with rack-and-pinion gears such that

$$f_{u,i} = \frac{\tau}{r} = \frac{i_{a,i}K_m}{r} \tag{2}$$

where K_m is the permanent magnet DC (PMDC) machine torque constant and r is the radius of the rack-and-pinion gear.

The linear motion of the wave is translated to rotational motion through the rack-and-pinion gear system. The linear velocity is converted to rotational velocity by the gear radius as

$$v_i = \dot{x}_i = rw_{m,i} \tag{3}$$

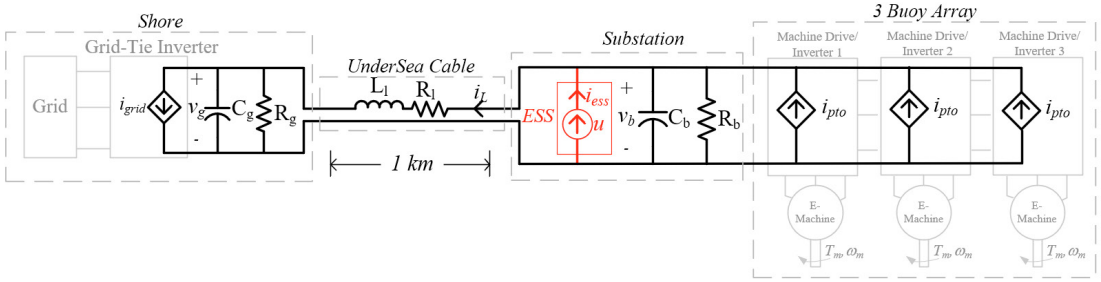

Fig. 2. Circuit model of a WEC connected to the grid (Weaver et al., 2020)

where v is the linear velocity that is converted to the rotational velocity, w_m, through the gear radius r. The rotational velocity then turns an electric machine on each of the buoys in the array.

2.2 Electrical Drive-Train

The electrical system on each of the buoys can be modelled by

$$\dot{i_{a,i}} = \frac{1}{L_a}(v_{a,i} - i_{a,i}R_a - \frac{K_m v_i}{r}). \tag{4}$$

The power injected into the electrical bus from each of the DC electric machines can be calculated as

$$i_{pto,i} = \frac{P_{pto,i}}{v_b} = \frac{v_{a,i}i_{a,i}}{v_b}. \tag{5}$$

The electric PTOs of the three electric machines are connected to an electric bus in parallel. The total current injected into the DC bus by the electric machines is

$$i_{ptosum} = \sum_{i=1}^{N} i_{pto,i}. \tag{6}$$

The electric bus is modelled in the circuit as a parallel RC circuit and ideal ESS. The electrical bus is connected to shore by a 1 km cable modelled by a series resistor and inductance. The grid connection is modelled by an RC circuit in parallel with a current source that represents the power delivered to the grid by the WEC. The electrical bus, line to shore, and grid can be modelled by the following

$$\dot{v_b} = \frac{1}{C_b}(i_{ptosum} - \frac{v_b}{R_b} - u - i_L) \tag{7}$$

$$\dot{i_L} = \frac{1}{L_L}(v_b - i_L R_L - v_g) \tag{8}$$

$$\dot{v_g} = \frac{1}{C_g}(i_L - i_{grid} - \frac{v_g}{R_g}) \tag{9}$$

where u is the ideal current from the ESS. The ideal current from the ESS can be calculated as

$$u = \frac{v_{sc} - v_b}{R_{ESR}}. \tag{10}$$

The variables for the mechanical system, the electric machine, and the electrical system can be found in Table 1.

2.3 Controls

The wave that is interacting with the WEC is modelled as the excitation force. The excitation force on the WEC array is generated by the wave climate the array is operating in. An irregular wave climate containing multiple

Table 1. System Parameter Descriptions

Parameter	Description	Units
m	Buoy Mass	kg
c	Buoy Damper Coefficient	$N/\frac{m}{s}$
k	Buoy Spring Coefficient	$\frac{N}{m}$
f_e	Wave Excitation Force	N
r	Rack and Pinion Gear Radius	m
v_a	PMDC Armature Voltage	V
i_a	PMDC Armature Current	A
K_m	PMDC Torque Constant	$\frac{Nm}{A}$
L_a	PMDC Armature Inductance	H
R_a	PMDC Armature Resistance	Ω
v_b	PTO Collection Bus Voltage	V
i_l	Line Current	A
v_g	Grid side Voltage	V
v_{sc}	ESS Voltage	V
i_{pto}	Current from Electric Machine Drive	A
i_{grid}	Current into Grid Inverter	A
u	Current from ESS	A
C_b	Bus Capacitance	F
R_b	Bus Parasitic Resistance	Ω
C_g	Grid Inverter Resistance	A
R_g	Grid Inverter Resistance	Ω
R_{ESR}	Equivalent Series Resistance of C_b	Ω

frequencies can be modelled as the sum of the individual frequency components

$$f_e = \sum_{n=1}^{N} A_n sin(w_n t + \phi_n). \tag{11}$$

When this multiple frequency excitation force interacts with the WECs the system reacts differently to each one of the multiple input frequencies. To extract the most energy from the WECs the excitation force must be decomposed into its individual frequencies, and a controller must be designed for each frequency.

The excitation force can be decomposed into its sub-components as

$$\hat{f_e}(t) = a_0 + \sum_{n=1}^{N}[a_n cos(n\omega t) + b_n sin(n\omega t)] \tag{12}$$

where a_0 is the average of $f_e(t)$, and a_n and b_n are the amplitudes of the sine and cosine components of one frequency in the decomposed signal. The amplitudes of the sine and cosine components are estimated using a Sequential Least Squares Estimator (SLSE) as

$$x_n = [a_1, b_1, ..., a_n, b_n]^T = x_{n-1} + PA^T(Y - Ax_{n-1}) \tag{13}$$

where P is the weighting matrix, A are the amplitudes of sine and cosine waves for a given frequency, Y is the measured values, and x_{n-1} is the previous amplitude estimate for the respective frequency component (Crassidis

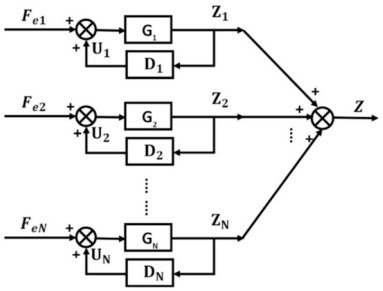

Fig. 3. Block diagram of the decomposed excitation force and PDC3.

and Junkins, 2004). Each of these components can be controlled using a PDC3 described in (Wilson et al., 2017; Song et al., 2016; Abdelkhalik et al., 2017b). PDC3 requires that the excitation force be decomposed into its individual frequencies and a PD controller be designed for each frequency. These individual control channels will then be summed up to create the control input for the complete excitation force. This process is shown in Fig. 3.

In PDC3 the proportional gain is designed so each channel of the controller will resonate with an individual frequency component of the decomposed excitation force and can be calculated as

$$k_{p,i} = \omega_i^2 m_i - k_i. \tag{14}$$

The derivative gain, k_d is chosen so that the real portion of the control impedance is equal to the real part of the mechanical impedance. The derivative gain is chosen as this in order to maximize the power out and to satisfy the complex conjugate control requirement

$$k_{d,i} = c_i. \tag{15}$$

The control signal from the PDC3 in this study is used to control the actuator of each of the WECs in the array. The multi-frequency sea state generating the excitation force on the WEC array can be described using a Bretschneider spectrum. The Bretschneider spectrum describes a sea state for a given significant wave height and peak frequency. The wave height and frequency data from the National Data Buoy Center, buoy number 46073 (US Department of Commerce NOAA, 1996), were used in addition with the Wave Analysis for Fatigue Oceanography (WAFO) toolbox to create the Bretschneider spectrum (Perez and Fossen, 2009). The values for the significant wave height and peak period are shown in Table 2. The spectrum was generated using the `Bretschneider` function from the WAFO toolbox. The frequency spectrum was converted to the time domain using the `spec2dat` function. The generated mean water level data was then scaled to resemble an excitation force acting upon the WEC. This force is shown in Fig. 5.

The PDC3 control method puts each WEC into resonance, or in other words, they will have a power factor of one. However, for regular waves each WEC will output power of the form

$$p_i(t) = cos^2(\omega_n t) = \frac{1}{2}(cos(2\omega_n t) + 1). \tag{16}$$

For a multi-wec array, each WEC power can be shifted in phase. If each WEC is shifted equally in phase ϕ, at a wave frequency of ω_n, then the power from each WEC is

$$p_i(t) = \frac{1}{2}(cos(2\omega_n t - 2(i-1)\phi) + 1) \tag{17}$$

Table 2. Bretschneider Spectrum Variables

Parameter	Description	Value
H_w	Significant Wave Height	2.2 m
T_s	Peak Period	9.2 s

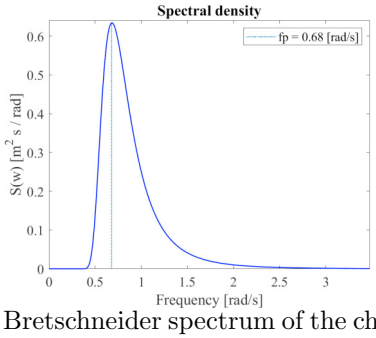

Fig. 4. The Bretschneider spectrum of the chosen sea state.

and the total sum of power from all N WECs is

$$P_{array} = \sum_{i=1}^{N} p_i(t) \tag{18}$$

$$= \frac{1}{2}(csc(\phi)sin(N\phi)cos(2\omega_n t + \phi(1-N))) + N). \tag{19}$$

The total sum of power will be constant if

$$csc(\phi)sin(N\phi) = 0 \tag{20}$$

which happens when

$$\phi \in \left\{ \frac{\pi}{N}, \frac{2\pi}{N} \right\}. \tag{21}$$

Therefore, the three WEC array will output a constant total power when the WECs are "phased" at $\pi/3rad = 60^o$ or $2\pi/3rad = 120^o$ apart in time (Husain et al., 2022). A constant power output leads to several advantages. The first is that there is minimal need for energy storage, the second is that the voltage ripple in the electrical collection buss is minimal, and third is that this also minimizes losses and improves power output to the grid. However, the inclusion of irregular waves with multiple frequencies and noise may not lead to constant power, but a minimum power variation can be found with proper phasing or time shifts between the WECs.

For the WEC array studied in this paper the forces of each of the three WECs are shifted in time to emulate a spacial separation along the direction of wave propagation as illustrated in Fig. 1. The wave forces for each of the three WECs used in this study are

$$f_{e,1}(t) = \hat{f}_e(t) \tag{22}$$

$$f_{e,2}(t) = \hat{f}_e(t - \Delta t) \tag{23}$$

$$f_{e,3}(t) = \hat{f}_e(t - 2\Delta t) \tag{24}$$

where Δt is the shift in time between the wave forces seen at the WEC. In this study Δt is a design parameter used to determine the optimal spacing of the WECs that will minimize power variations.

3. SIMULATION RESULTS

The excitation force in the MATLAB/Simulink model was a wave force developed from the Bretschneider Spectrum. The toolbox that was used to create this spectrum is described in Section 2. The excitation force was then

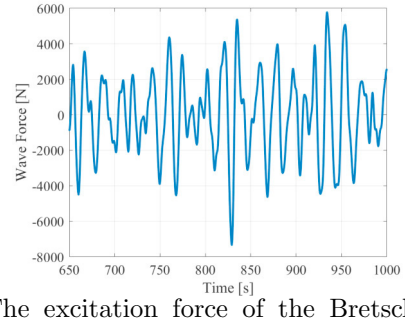

Fig. 5. The excitation force of the Bretschneider wave $\hat{f}_e(t)$.

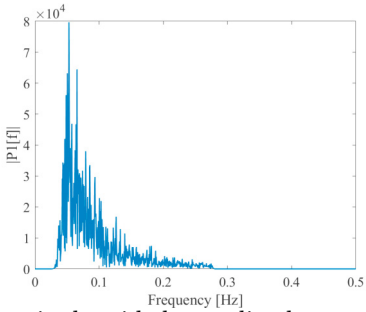

Fig. 6. The single sided amplitude spectrum of the Bretschneider wave excitation force.

Table 3. Frequency Channels used in PDC3 Controller

Channel	Frequency (Hz)
1	0.053
2	0.0505
3	0.0655
4	0.0485

transformed from the time domain into the frequency domain using MATLAB's built in Fast Fourier Transform (FFT) function. The Fourier Transform of the excitation force is shown in Fig. 6. The Fourier Transform of the excitation force was used to determine the peak frequencies in the excitation force. The top four frequency components in the excitation force were chosen to tune the proportional gain in each of the four PDC3 channels. These frequencies can be viewed in Table 3. These four frequencies are used in the SLSE described in Section 2 of this paper to estimate the amplitudes of each of these four frequencies in the total Bretschneider excitation force.

In the first simulation one WEC was simulated and the number of PDC3 control channels enabled was varied from one to all four channels. In this case the proportional gains of each of the channels were tuned to the four top frequencies in the excitation force. Adding in additional channels to the controller increases the buoy's resonance with the multi-frequency Bretschneider excitation force. Increasing the resonance of the buoy with the excitation force increases the energy absorption of the buoy which increases the PTO power produced by the WEC. The PTO power that is produced by the WEC is then sent to the onshore electrical grid via the undersea cable where it is then injected into the grid. The grid power in the system is positive because the grid is consuming the power that is generated by the PTO. The power that is extracted with one PDC3 channel enabled is small due to the fact

Table 4. Average PTO and Grid Power for PDC3 Channels Enabled

Channels	PTO Power [W]	Grid Power [W]
1	267.5	27.2
2	527.7	258.6
3	566.5	300.8
4	672.4	412.1

Table 5. Results Varying Time Shifts on the 3 WECs

Δt [s]	Pk-Pk Voltage Noise [%]	ESS Energy [kJ]	Grid Power [kW]
0	5.20	76.5	1.8
1	3.63	61.3	1.77
2	1.50	44.5	2.14
3	0.80	29.8	1.47
4	1.44	38.6	1.77
5	2.43	29.4	2.13
6	3.04	42.8	2.33

that the buoy does not resonate well with the multi-frequency Bretschneider excitation force when the control force is generated from the estimate of only one frequency component. A summary of the PTO and Grid Powers extracted using 4 channels is summarized in Table 4.

The model was then extended to include three WECs operating in the Bretschneider sea state. Each of the three WECs had a PDC3 with four frequency channels. The time shift between each of the WECs was adjusted in 1 second increments to span the space to determine the optimal positional phasing. Changing the spatial position of the WECs relative to each other in the water changes the phasing of the excitation force interacting with each WEC. A phase change in the excitation force interacting with the WEC results in a phase change of the PTO current which can be utilized to minimize the noise in the bus voltage and minimize the size of the ESS. The difference in the bus voltage noise is also shown in Fig. 7. The difference in the maximum energy stored in the ESS for varying phase shifts of the three WECs is plotted in Fig. 8. The power exported to the grid versus the time shift between the three WECs is plotted in Fig. 9. A summary of the voltage noise, ESS Energy and Exported Grid Power is given in Table 5.

The results summarized in Table 5 show that the operation produces advantages results slightly before $\Delta t = 3s$, which gives low noise, a decreased ESS size and increased power exported to the gird. In this study the fundamental frequency from Table 3 is 0.053 Hz or a period of 18.86 s. A 60^o phase shift would be equivalent to $\frac{18.86\ s}{6} = 3.1\ s$. The 0.053 Hz channel used for the PDC3 controller is where the majority of the wave energy is contained (shown in Fig. 6). Other frequency content from the Bretschneider spectrum also adds to the energy harvesting and the phase of each frequency band may contribute to the array constant power effect.

4. CONCLUSION

This paper implements PDC3 on a WEC and shows that adding additional frequency control channels increases the buoys resonance with the multi-frequency excitation force and increases the WECs EPG power output. The PDC3 was then implemented on an array of 3 WECs as well as power packet phase control through the physical spacing

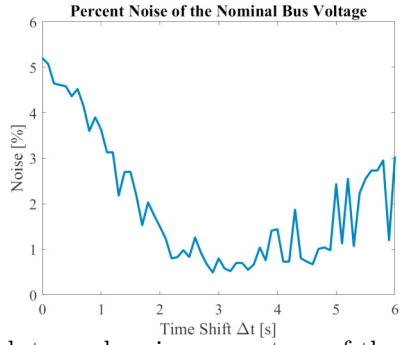

Fig. 7. Peak-to-peak noise percentage of the nominal bus voltage versus time shifts.

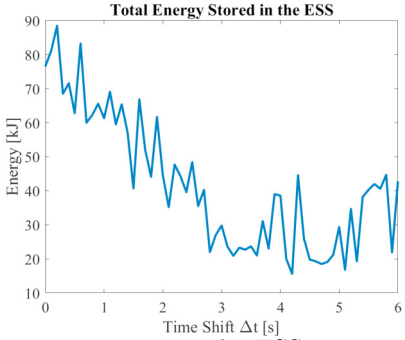

Fig. 8. Maximum energy in the ESS versus time shifts.

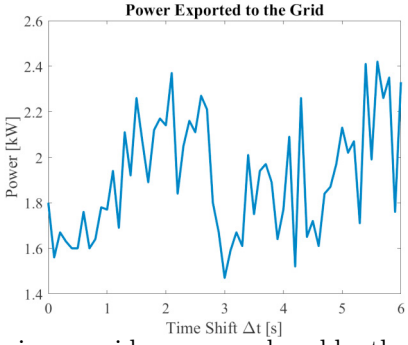

Fig. 9. Maximum grid power produced by the three WECs versus time shifts.

of the 3 WECs. The physical spacing caused a phase shift in the electrical signals from each buoy. It was shown that a time shift of slightly less than 3 seconds produced decreased noise, the decreased ESS energy, and increased the power exported to the grid. The phase control of 60^o identified the range the optimal results would be in but due to additional frequency components in the spectrum the optimal results were not located exactly at 60^o. Future work will include large clusters of WEC arrays that receive predictive forecasts that are optimized in a supervisory energy management system for effective performance.

REFERENCES

Abdelkhalik, O., Zou, S., Robinett, R.D., Bacelli, G., Wilson, D.G., Coe, R., and Korde, U. (2017a). Multiresonant feedback control of a three-degree-of-freedom wave energy converter. *IEEE Transactions on Sustainable Energy*, 8(4), 1518–1527.

Abdelkhalik, O., Zou, S., Robinett, R.D., Bacelli, G., Wilson, D.G., Coe, R., and Korde, U. (2017b). Multiresonant feedback control of a three-degree-of-freedom wave energy converter. *IEEE Transactions on Sustainable Energy*, 8(4), 1518–1527.

Bacelli, G. (2014). *Optimal control of wave energy converters*. National University of Ireland, Maynooth (Ireland).

Chen, M. and Poor, H.V. (2020). High-frequency power electronics at the grid edge: a bottom-up approach toward the smart grid. *IEEE Electrification Magazine*, 8(3), 6–17.

Copping, A.E., Green, R.E., Cavagnaro, R.J., Jenne, D.S., Greene, D., Martinez, J.J., and Yang, Y. (2020). Powering the blue economy-ocean observing use cases report. Technical report, Pacific Northwest National Lab.(PNNL), Richland, WA (United States).

Crassidis, J.L. and Junkins, J.L. (2004). *Optimal estimation of dynamic systems*. Chapman and Hall/CRC.

Falnes, J. and Kurniawan, A. (2020). *Ocean waves and oscillating systems: linear interactions including wave-energy extraction*, volume 8. Cambridge university press.

Fusco, F. and Ringwood, J.V. (2012). A simple and effective real-time controller for wave energy converters. *IEEE Transactions on sustainable energy*, 4(1), 21–30.

Husain, S., Parker, G.G., and Weaver, W.W. (2022). Storage minimization of marine energy grids using polyphase power. *Journal of Marine Science and Engineering*, 10(2), 219.

Jacobson, P.T., Hagerman, G., and Scott, G. (2011). Mapping and assessment of the united states ocean wave energy resource. Technical report, Electric Power Research Institute.

Perez, T. and Fossen, T.I. (2009). A MATLAB toolbox for parametric identification of radiation-force models of ships and offshore structures.

Song, J., Abdelkhalik, O., Robinett, R., Bacelli, G., Wilson, D., and Korde, U. (2016). Multi-resonant feedback control of heave wave energy converters. *Ocean Engineering*, 127, 269–278.

Takahashi, R., Azuma, S.i., and Hikihara, T. (2016). Power regulation with predictive dynamic quantizer in power packet dispatching system. *IEEE Transactions on Industrial Electronics*, 63(12), 7653–7661.

US Department of Commerce NOAA (1996). NDBC station page. URL `https://www.ndbc.noaa.gov/station_page.php?station` = 46073. *Accessed* : 2021/11/06.

Veurink, M.G., Weaver, W.W., Wilson, D.G., Robinett, R.D., and Matthews, R.C. (2022). Wave energy converter optimization with multi-resonance controller of the electrical power take-off. In *IEEE Power and Energy Conference at Illinois (PECI)*, 1–6. IEEE.

Weaver, W.W., Wilson, D.G., Hagmuller, A., Ginsburg, M., Bacelli, G., Robinett, R.D., Coe, R., and Gunawan, B. (2020). Super capacitor energy storage system design for wave energy converter demonstration. In *IEEE International Symposium on Power Electronics, Electrical Drives, Automation and Motion*, 564–570.

Wilson, D.G., Bacelli, G., Robinett, R.D., Korde, U.A., Abdelkhalik, O., and Glover, S.F. (2017). Order of magnitude power increase from multi-resonance wave energy converters. In *OCEANS*, 1–7. IEEE.

Wilson, D.G., Weaver, W.W., Bacelli, G., and Robinett, R.D. (2018). Wec array electro-mechanical drivetrain networked microgrid control design and energy storage system analysis. In *2018 International Symposium on Power Electronics, Electrical Drives, Automation and Motion (SPEEDAM)*, 1278–1285. IEEE.